Bioprocess and Biosystems Engineering (2020) 43:1499–1508
https://doi.org/10.1007/s00449-020-02343-3

RESEARCH PAPER

Antibacterial activities of zinc oxide and Mn-doped zinc oxide synthesized using *Melastoma malabathricum* (L.) leaf extract

Mohammad Mansoob Khan[1] · Mohammad Hilni Harunsani[1] · Ai Ling Tan[1] · Mirabbos Hojamberdiev[2] · Syafiqah Azamay[3] · Norhayati Ahmad[3]

Received: 25 October 2019 / Accepted: 3 April 2020 / Published online: 19 April 2020

Abstract
Zinc oxide (ZnO) is considered as a potential antimicrobial agent. This work aims to investigate the properties of ZnO and Mn-doped ZnO (1% and 5%) fabricated using aqueous leaf extract of *Melastoma malabathricum* via green synthesis and its antibacterial activities. The synthesized ZnO and Mn-doped ZnO were characterized using different techniques such as powder X-ray diffraction, scanning electron microscopy, X-ray photoelectron spectroscopy and UV–Vis diffuse reflectance spectroscopy. The synthesized ZnO and Mn-doped ZnO were tested for its antibacterial properties on two Gram-negative bacteria: *Escherichia coli* and *Pseudomonas aeruginosa*, and two Gram-positive bacteria: *Bacillus subtilis* and *Staphylococcus aureus*. The results showed positive antibacterial effects for *B. subtilis* and *S. aureus* only. Among the three materials tested, 1% Mn-doped ZnO exhibited the highest antibacterial activity for *B. subtilis* with the minimum inhibitory concentration being 50 mg/mL.

Keywords ZnO · Zinc oxide · Metal oxides · Mn-doped ZnO · Green synthesis · Leaf extracts · *Melastoma malabathricum* · Antibacterial · Antimicrobial

Introduction

Zinc oxide nanoparticles (ZnO NPs) are of interest as favorable antimicrobial agent due to its high resistance to heat denaturation, low decomposability and slightly longer usable lifespan in comparison to other organic antimicrobial agents [1]. ZnO has been shown to possess good antibacterial property against both Gram-positive and Gram-negative bacteria partially due to its reactive oxygen species (ROS) producing effect which had been researched to be cytotoxic towards bacterial cells [2, 3]. One of the properties of ZnO NPs which may be responsible for the high antimicrobial activity is the low-energy band gap [4]. This property allows for an above average production of reactive oxygen species when the ZnO interacts with the biomolecules [5].

The properties of ZnO can be slightly altered to a more favorable characteristic to produce ZnO powder that is more efficient against bacterial activity [6]. One of the ways this can be achieved is by doping with a different material. In the event that Mn-doped ZnO has a higher stability, the cytotoxic effect of the ZnO NPs may be lowered as the Mn doping may decrease the dissociation time of ZnO NPs. A more gradual dissociation of ZnO can result in a lower risk of an exponential increase of ROS and this phenomena favors the use of ZnO powder as an antiseptic cream on human skin [7]. Furthermore, the particle size of Mn-doped ZnO NP has been shown to be smaller in comparison to undoped ZnO NP, hence making it more effective in influencing the cell systems [8, 9].

Previous reports have also suggested that the crystalline structure and particle shape of the ZnO have less influence on the antimicrobial ability as compared to the particle size [10]. There are implications that negatively charged NPs are

✉ Mohammad Mansoob Khan
mmansoobkhan@yahoo.com; mansoob.khan@ubd.edu.bn

[1] Chemical Sciences, Faculty of Science, Universiti Brunei Darussalam, Jalan Tungku Link, Gadong BE 1410, Brunei Darussalam

[2] Fachgebiet Keramische Werkstoffe/Chair of Advanced Ceramic Materials, Institut für Chemie, Technische Universität Berlin, Straße des 17, Juni 135, 10623 Berlin, Germany

[3] Environmental & Life Sciences, Faculty of Science, Universiti Brunei Darussalam, Jalan Tungku Link, Gadong BE 1410, Brunei Darussalam

more effective for biological applications due to their higher adsorption rate; whereas, a positively charged NP would aid in reducing the toxicity of particle [11].

The green approach is where the biochemical compounds present in the organic extract can act as reducing agents in the synthesis or help the stabilization of the metal oxide NPs [12]. Biosynthesized nanoparticles also showed better antimicrobial action in comparison to its chemically synthesized counterpart as the green-synthesized ZnO has a stronger inhibitory effect [11]. The green-synthesized ZnO NPs showed relatively low toxicity as the toxic chemical that may appear in the chemical synthesis had been replaced by a non-toxic phytochemical [13–16].

In this work, the green synthesis of ZnO employed the use of aqueous leaf extract from the plant, *Melastoma malabathricum* locally known in Brunei as 'kuduk-kuduk' (Fig. 1). This plant is native to Southeast Asia and belongs to the *Melastomataceae* family where it was previously reported to exhibit antiviral, cytotoxic and a high anti-oxidant activity [17, 18].

Herein, we report the first fabrication of ZnO and Mn-doped ZnO using the aqueous leaf extract of *Melastoma malabathricum*. The fabricated ZnO and Mn-doped ZnO NPs were characterized and tested for antibacterial activities against four bacterial strains.

Materials and methods

Materials, techniques and methods used

$Zn(NO_3)_2{\cdot}6H_2O$ (98%) and $Mn(CH_3CO_2)_2{\cdot}4H_2O$ were purchased from Sigma-Aldrich and used as received. *Melastoma malabathricum* (*L.*) leaves were obtained from Universiti Brunei Darussalam Botanical Research Centre (UBD BRC) and authenticated by a botanist from UBD BRC.

Powder X-ray diffraction (XRD, MiniflexII, Rigaku, Japan) analysis was carried out to determine the structural properties and phase purity of the fabricated ZnO and Mn-doped ZnO using Cu Kα radiation. The optical properties of the fabricated materials were examined using ultraviolet–visible (UV–Vis) diffuse reflectance spectroscopy (UV-3600 UV–Vis NIR Spectrophotometer, Shidmadzu, Japan). The chemical states and surface analysis of the fabricated ZnO and Mn-doped ZnO NPs was performed using X-ray photoelectron spectroscopy (XPS, JPS-90110MC, JEOL, Japan). The C 1 s (285 eV) was used as a reference to calibrate the peak positions of the elements. The morphology, particle size and composition were measured using scanning electron microscopy (SEM, JEOL, Japan). The fabricated ZnO and Mn-doped ZnO were also analyzed for surface charge (zeta potential) using Malvern Zetasizer Nano series.

Fig. 1 *Melastoma malabathricum* plant used for the synthesis of ZnO

Preparation of the aqueous leaf extract

The leaves of the *Melastoma malabathricum* (*L.*) were collected and washed to remove dust and residues. Leaves were air dried overnight before being finely cut and then ground into a thick paste. The thick paste weighing 5 g was then mixed with 100 mL of distilled water in a 250-mL beaker. The mixture was left to be stirred for 1 h before the leaf extract was obtained using gravity filtration.

Synthesis of undoped ZnO and (1% and 5%) Mn-doped ZnO

For the fabrication of undoped ZnO NPs, $Zn(NO_3)_2{\cdot}6H_2O$ as a precursor was added into 30 mL of aqueous leaf extract. The solution mixture was preheated to 60 °C and then stirred at constant temperature until a paste was formed. The paste was transferred into a crucible and it was calcined at 400 °C for 2 h. The product was ground into fine powder and kept in a desiccator for further characterization and application.

For the synthesis of Mn-doped ZnO, the same procedure was followed but with an addition of $Mn(CH_3CO_2)_2{\cdot}4H_2O$ as a second precursor. The $Mn(CH_3CO_2)_2{\cdot}4H_2O$ was added immediately after the addition of $Zn(NO_3)_2{\cdot}6H_2O$ into the extract solution. The same procedure was carried out throughout the experiment. The product obtained was ground into fine powder and kept in a desiccator for characterization and application.

Antibacterial activity screening

The microorganisms used in this study consisted of four bacterial strains, two Gram-negative bacteria: *Escherichia coli* (ATCC 25922) and *Pseudomonas aeruginosa* (ATCC 27853) and two Gram-positive bacteria: *Bacillus subtilis* (ATCC 6633) and *Staphylococcus aureus* (ATCC 25923). The antibacterial activities of the green-synthesized ZnO were determined by disc diffusion method.

The samples were first screened for anti-microbial activity at the highest concentration (500 mg/mL). 10 µL of biosynthesized ZnO, 1% Mn-doped ZnO and 5% Mn-doped ZnO was applied onto a 6-mm Whatman No.1 filter paper disc and was left to dry overnight. They were then placed on a spread of bacterial lawn on a Mueller–Hinton agar (MHA) plate alongside one negative and two positive controls (Fig. 2a). The positive controls used consisted of 500 mg/mL commercial ZnO and 20 mg/mL Streptomycin. The negative control used was 10 mL of distilled water. The zone of inhibition was recorded after incubating the plates at 37 °C for 24 h. Each test was carried out in triplicates.

Minimum inhibitory concentration

The minimum inhibitory concentration (MIC) testing of the samples was carried out on the bacterial strains that have shown activity (inhibition zone of > 7 mm) from the previous antibacterial tests screening. Five concentrations of each sample were prepared at lower concentrations (25, 50, 100, 300 and 500 mg/mL) and 10 µL of each concentration of the sample was loaded onto paper disc to be placed onto Mueller–Hinton agar plate together with the positive and negative controls (Fig. 2b). The plate was incubated overnight at 37 °C and the zone of inhibition was measured by diameter comparison after 24 h. The experiments were performed in triplicates with fresh bacterial inoculum.

Results and discussion

Using green and phytogenic approach, we report that undoped ZnO, 1% and 5% Mn-doped ZnO were successfully fabricated using the aqueous leaf extract of *Melastoma malabathricum* (*L.*). The advantage of this approach is that it is simple, environmentally friendly, and it does not require any harmful chemicals, high-energy inputs, capping or reducing agents and lengthy treatments. The reaction medium for this protocol was water and the fabrication process took place at low temperature, 30–60 °C, except calcination of the paste at 400 °C.

Powder X-ray diffraction

The powder XRD analysis was conducted to determine the purity, structure and crystallite size of the ZnO and Mn-doped ZnO. Figure 3a shows the XRD patterns obtained from the undoped ZnO, Mn-doped ZnO and commercial ZnO (ZnO–C) samples. The diffraction peaks correspond to (100), (002), (101), (102), (110) and (103) crystal planes of the wurtzite crystal structure of ZnO NPs (JCPDS-36–1451), and no additional features from impurities and residues were detected, suggesting that the fabricated ZnO NPs are of single-phase ZnO without impurities. These results confirmed that the undoped ZnO and Mn-doped ZnO have been successfully synthesized. The absence of Mn oxide peaks suggests that Mn has been inserted into the lattice and the samples are pure. The mean crystallite size of the nanoparticles was calculated using Scherrer's equation and was found to be 4.75 nm, 4.36 nm and 4.62 nm for undoped ZnO, 1% Mn-doped ZnO and 5% Mn-doped ZnO, respectively.

UV–Vis DRS studies

To examine the effects of Mn-doping on the optical properties, the undoped ZnO, 1% and 5% Mn-doped ZnO were analyzed using UV–Vis DRS spectroscopy within the wavelength range of 200–800 nm. Figure 3b presents the UV–Vis DRS absorbance spectra of ZnO–C and undoped ZnO as well as 1% and 5% Mn-doped ZnO NPs. From the spectra, the absorbance of ZnO–C was observed at ~ 390 nm. Whereas absorbance for undoped ZnO, 1% and 5% Mn-doped ZnO showed a red shift. In comparison to the ZnO–C, the biosynthesized ZnO also showed high absorbance in the range 500–800 nm. The approximate band gap energy was calculated by inputting the absorption peak values (λ) in the following equation:

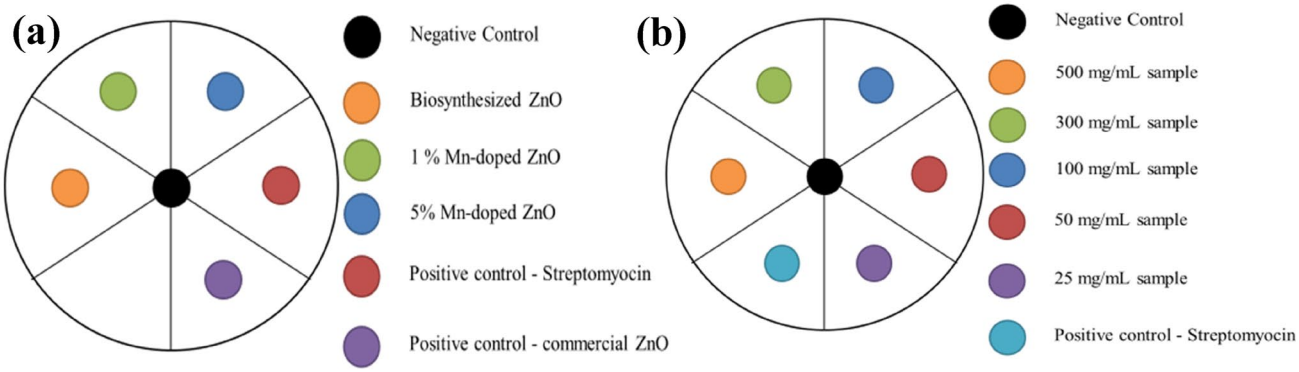

Fig. 2 Zone of inhibition for **(a)**, antibacterial activity and **(b)** MIC screening on MHA plate

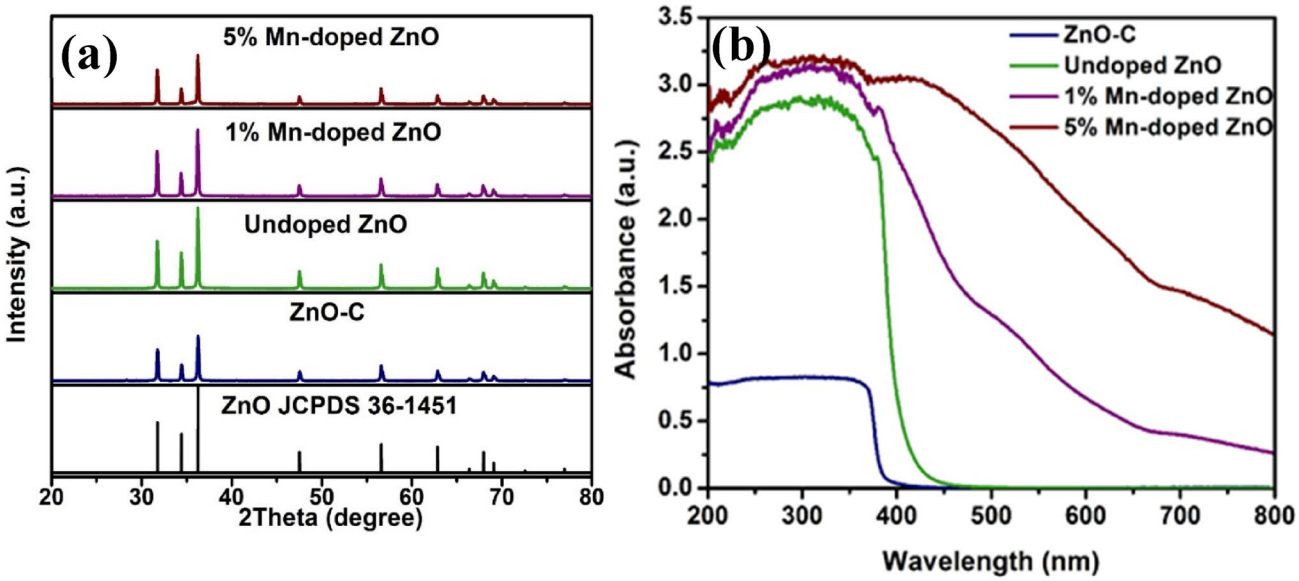

Fig. 3 XRD patterns **(a)**, and UV–Vis DRS spectra of ZnO–C and undoped ZnO as well as 1% and 5% Mn-doped ZnO Zeta Potential measurements **(b)**

$$E_g = \frac{hc}{\lambda} \quad (1)$$

where h is Planks constant (6.626×10^{-34} Js), c is the speed of light (3.0×10^{8} ms^{-1}) and λ is wavelength (nm). The approximate band gap energy was found to be 3.06 eV for ZnO, 2.66 eV for 1% Mn-doped ZnO and 2.56 eV for 5% Mn-doped ZnO. The synthesized ZnO and Mn-doped ZnO samples have lower band gap energy values in comparison to the ZnO–C (3.18 eV). The 5% Mn-doped ZnO has the lowest band gap energy compared to the other two synthesized ZnO.

Surface charge of nanoparticles is an important factor that influences cell membrane interaction. In this work, the zeta potential of the fabricated ZnO surface charge was investigated using Malvern Zetasizer Nano series. The zeta potential for the undoped ZnO NP, 1% Mn-doped ZnO and 5% Mn-doped ZnO was found to be − 0.15 mV, 2.32 mV and 2.22 mV, respectively (Table 1). This indicates that there is a net positive surface charge for 1% Mn-doped ZnO and 5% Mn-doped ZnO; whilst, the undoped ZnO had a negative surface charge. This suggests that the Mn doping can affect the surface charge of ZnO, although the values obtained for the 1% and 5% Mn were similar to each other.

Table 1 Zeta potential of undoped ZnO, 1% Mn-doped ZnO and 5% Mn-doped ZnO

Sample	Reading	Zeta potential (mV)
Undoped ZnO	1	− 0.04
	2	− 0.18
	3	− 0.23
	Average	− 0.15 (±0.10)
1% Mn-doped ZnO	1	1.65
	2	2.43
	3	2.88
	Average	2.32 (±0.62)
5% Mn-doped ZnO	1	2.11
	2	2.51
	3	2.06
	Average	2.22 (±0.30)

Scanning electron microscopy and energy-dispersive X-ray spectroscopy

The SEM images suggested that the fabricated ZnO showed a roughly spherical shape. Figure 4a illustrates an agglomerated spherical shape of the synthesized nanoparticles [19]. The morphology of the 1% Mn-doped ZnO was spherical-shaped NPs as illustrated in Fig. 4b. Based on Fig. 4, the sizes of the NPs were calculated to be approximately 272 nm, 705 nm and 222 nm for ZnO, 1% Mn-doped ZnO and 5% Mn-doped ZnO, respectively. The inset in each figure shows the respective EDX spectra that confirmed the presence of zinc, oxygen in all three samples and manganese in Mn-doped ZnO samples as presented in Fig. 4b, c. Few other low-intensity peaks were also observed in the EDX spectra. These peaks indicate the presence of elements, such as carbon and potassium which could be originated from the leaf extract. It was reported that these phytochemicals from leaf extract are involved in the reduction and capping of the ZnO [20].

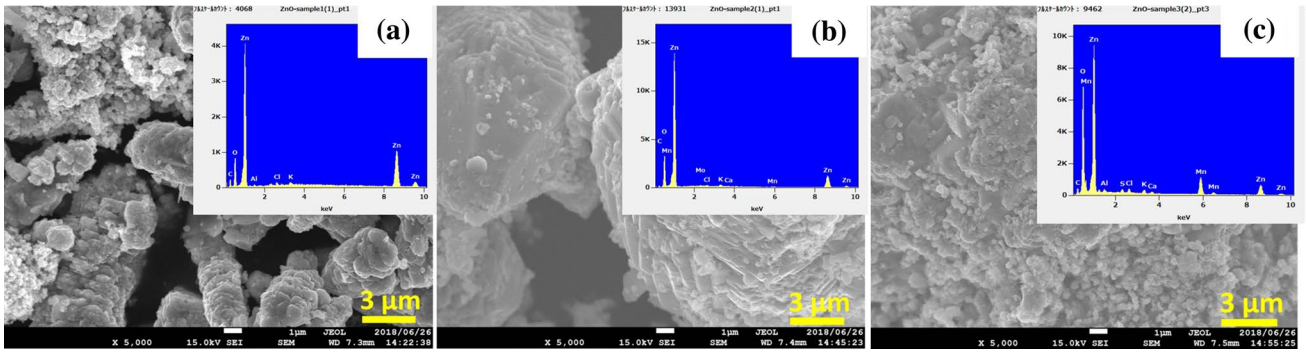

Fig. 4 SEM images of **(a)**, undoped ZnO, **(b)**, 1% Mn-doped ZnO and **(c)** 5% Mn-doped ZnO and the inset shows their respective EDX

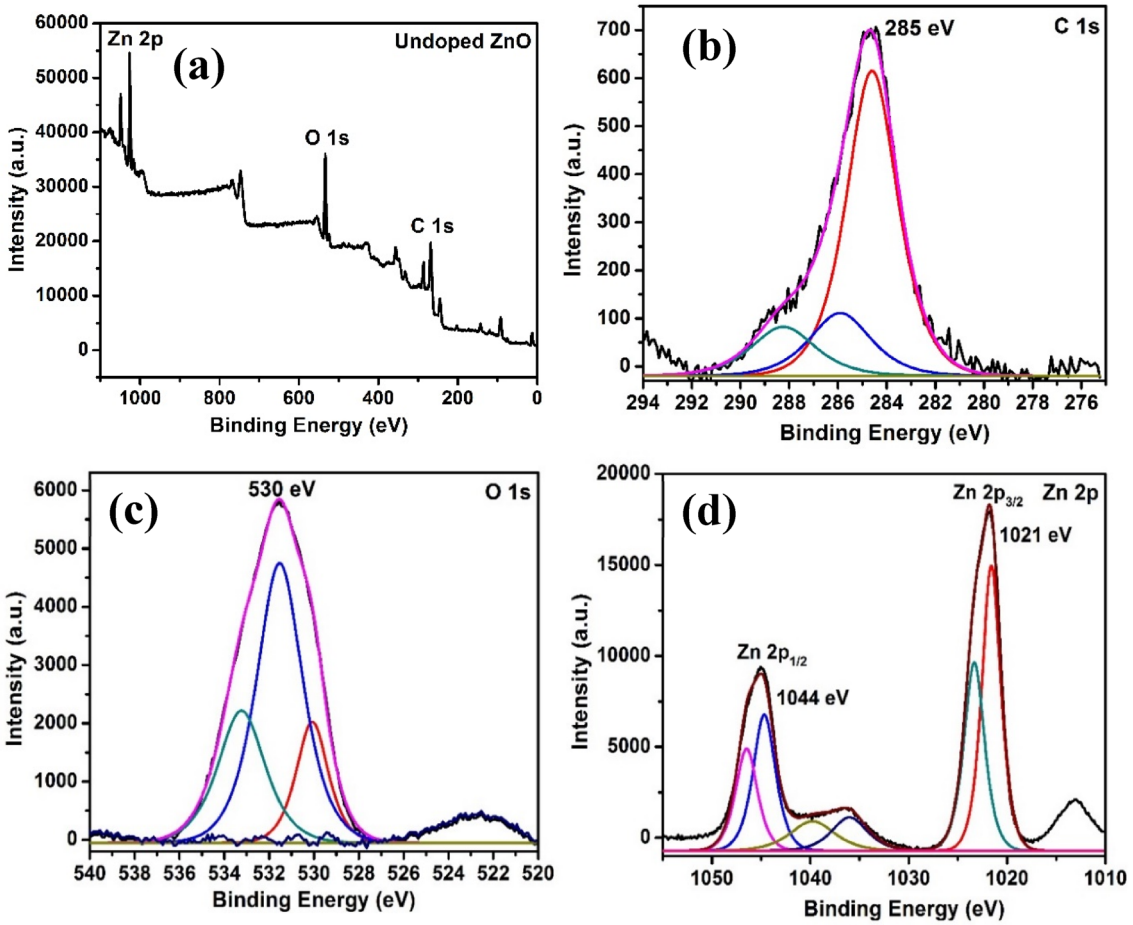

Fig. 5 Deconvoluted XP spectra of the undoped ZnO **(a)**, survey, **(b)**, C 1 s, **(c)**, O 1 s, and, **(d)** Zn 2p

X-ray photoelectron spectroscopy analysis

XPS was used to quantitatively analyze and examine the bonding, chemical states and surface chemical composition of the undoped ZnOs. Figure 5a shows the survey spectrum of the fabricated undoped ZnO that displays all the expected elements which correspond to Zn 2p, O 1 s and C 1 s. This suggests that there were no impurities in the undoped ZnO. Figure 5b shows the C 1 s photoelectron peak at a binding energy (BE) of 285 eV, which was attributed to the surface

carbon impurities. The carbon element represents the phytochemical compounds of the leaf extract present on the surface of the samples. The chemical states of O were examined, and XP spectrum of O 1 s of the undoped ZnO NPs are shown in Fig. 5c. The O 1 s spectrum of the ZnO was fitted with three peaks which may be present in different oxygen environments, the presence of loosely bound oxygen on the surface of ZnO, O^{2-} ions in the wurtzite structure of hexagonal Zn^{2+} ions and O^{2-} in the oxygen-deficient regions within the ZnO matrix [16]. Figure 5d shows Zn 2p spectrum resulted in two peaks at binding energies of 1021 eV and 1044 eV which corresponds to the Zn^{2+} $2p_{3/2}$ and Zn^{2+} $2p_{1/2}$, respectively, indicating that Zn in the undoped ZnO is in the form of Zn^{2+} [16].

Figure 6 shows XP spectra of the 5% Mn-doped ZnO. Figure 6a shows the survey spectrum of the fabricated 5% Mn-doped ZnO that displays all the expected elements which

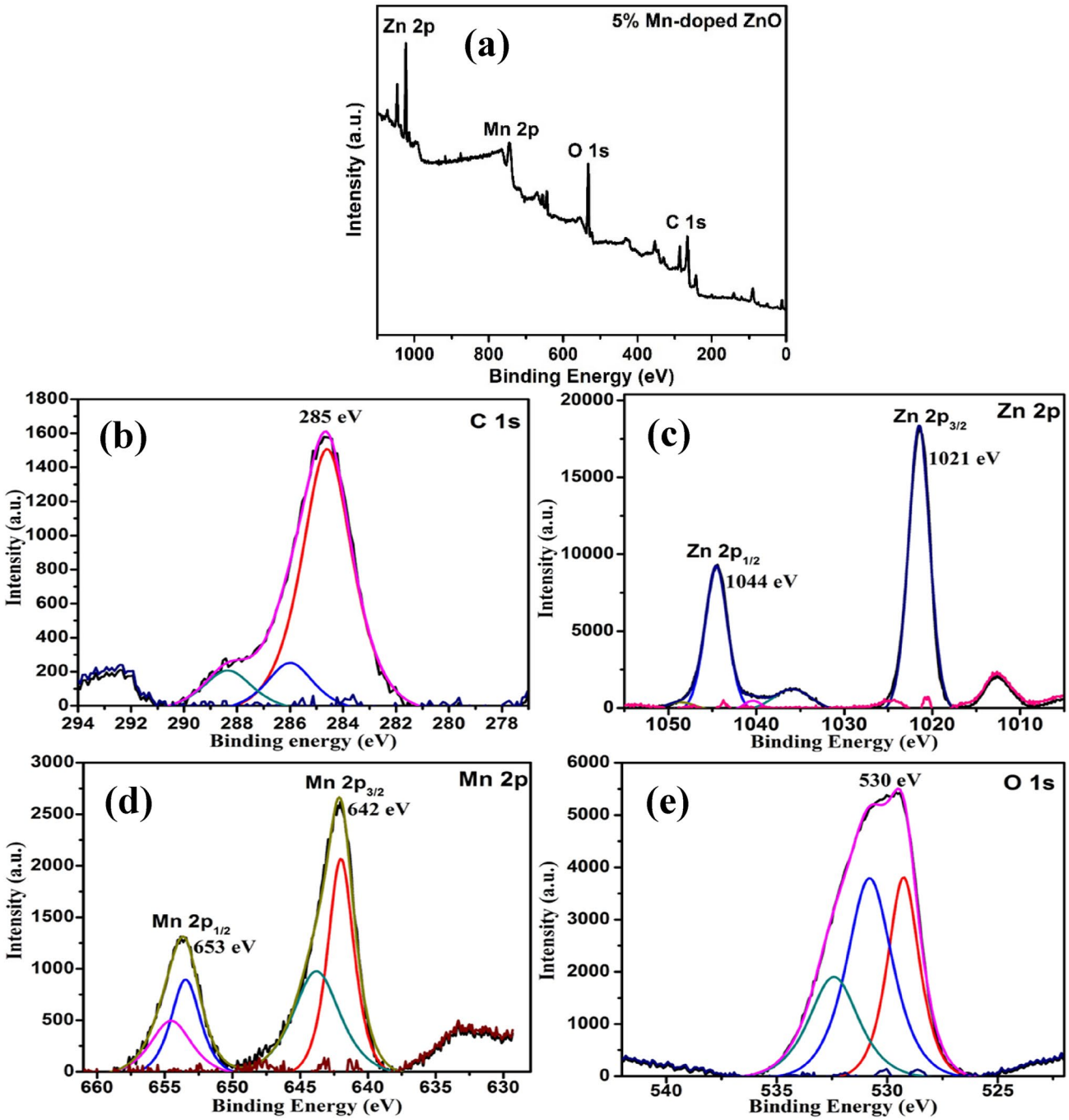

Fig. 6 Deconvoluted XP spectra of the 5% Mn-doped ZnO of **(a)**, survey spectra, **(b)**, C 1 s, **(c)**, Zn 2p, **(d)**, Mn 2p, and, **(e)** O 1 s

correspond to Zn 2p, Mn 2p, O 1 s and C 1 s. Figure 6b shows the C 1 s photoelectron peak at a binding energy (BE) of 285 eV, which was attributed to the surface carbon impurities. The carbon element represents the phytochemical compounds of the leaf extract present on the surface of the samples. Figure 6c shows the Zn 2p spectrum in which two peaks at binding energies of 1021 eV and 1044 eV correspond to the photo-splitting electrons, Zn^{2+} $2p_{3/2}$ and Zn^{2+} $2p_{1/2}$, respectively, indicating that Zn in the sample is in the form of Zn^{2+}. Figure 6d shows the Mn 2p spectrum with two peaks at binding energy 642 eV and 653 eV which corresponds to the Mn^{2+} $2p_{3/2}$ and Mn^{2+} $2p_{1/2}$ respectively. To determine the binding states of oxygen in 5% Mn-doped ZnO, the O 1 s XPS peak was fitted to three peaks centered at BE of 530.52, 532.22 and 528.06 eV. Figure 6e shows the chemical states of O in the 5% Mn-doped ZnO. The O 1 s spectrum of the ZnO can be ideally thought of as being comprised of three factors: the presence of loosely bound oxygen on the surface of ZnO, O^{2-} ions in the wurtzite structure of hexagonal Zn^{2+} ions and O^{2-} in the oxygen-deficient regions within the ZnO matrix [16].

Antibacterial activity screening

The in vitro antimicrobial activity of the ZnO, 1% Mn-doped ZnO and 5% Mn-doped ZnO fabricated using *Melastoma malabathricum* aqueous leaf extract was evaluated against two Gram-negative bacteria (*E. coli* and *P. aeruginosa*) and two Gram-positive bacteria (*B. subtilis* and *S. aureus*). The antibacterial screening shows that *P. aeruginosa* and *E. coli* tests did not exhibit any zone of inhibitions at the maximum concentration of 500 mg/mL tested (Table 2). This could be due to the bacteria having a metallostasis mechanism that can enable it to thrive in Zn-excess and Zn-depleted condition. The mechanism in *P. aeruginosa* involves a zinc uptake regulator (ZUR) protein which regulates the Zn content in the cell [21]. Furthermore, *P. aeruginosa* has protein pumps such as the CzcCBA efflux pump which plays an essential role in the resistance to heavy metal and lowering the risk of metal intoxication. Hence, the overall effect of Zn^{2+} ions toxicity mechanism suggests that it is nullified in these bacteria.

However, all the green-synthesised ZnO reported here showed antibacterial activity against *B. subtilis* and *S. aureus* at the highest concentration tested at 500 mg/mL. No inhibition zone was detected for the negative control in all the tests.

Minimum inhibitory concentration

The MIC was performed on ZnO, which upon screening, was found to have a medium to high zone of inhibition of at least 7 mm. The results for the MIC tests of *B. subtilis* and *S. aureus* with the undoped and Mn-doped ZnO samples are shown in Figs. 7 and 8. There was no zone of inhibition

Table 2 Mean results of the antibacterial screening activities for bacteria: *S. aureus, B. subtilis*, *E. coli* and *P. aeruginosa* against commercial, undoped ZnO and Mn-doped ZnO at maximum concentration of 500 mg/mL

Bacteria strain	Average (±SD) zone of inhibition/mm				
	Undoped ZnO (500 mg/mL)	1% Mn-doped ZnO (500 mg/mL)	5% Mn-doped ZnO (500 mg/mL)	Commercial ZnO (500 mg/mL)	Streptomycin (20 mg/mL)
B. subtilis	9.50 (±0.87)	12.00 (±0.00)	10.70 (±0.58)	10.50 (±1.32)	34.00 (±1.00)
S. aureus	8.70 (±1.26)	10.8 (±2.25)	10.80 (±1.04)	10.20 (±0.29)	25.30 (±0.58)
E. coli	–	–	–	–	25.30 (±1.53)
P. aeruginosa	–	–	–	–	27.00 (±1.33)

The (–) symbol represents negative screening result

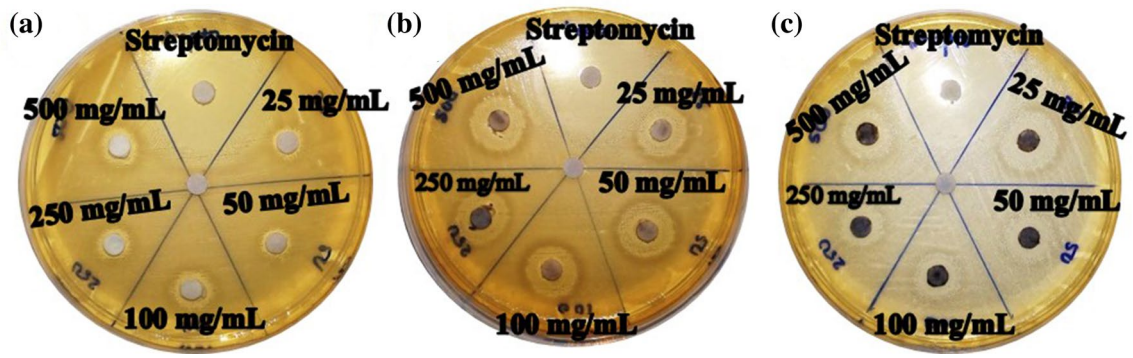

Fig. 7 Results for *B. subtilis* MIC screening tests for **(a)**, undoped ZnO, **(b)**,1% Mn-doped ZnO and **(c)** 5% Mn-doped ZnO

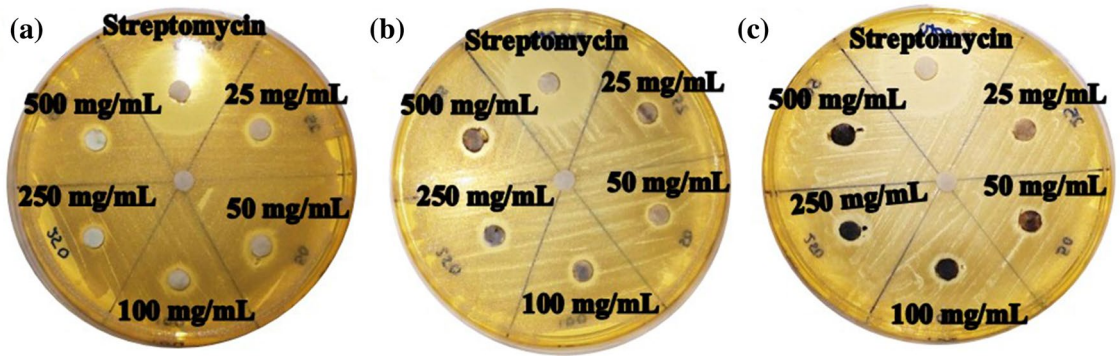

Fig. 8 Results for *S. aureus* MIC screening tests for **(a)**, undoped ZnO, **(b)**, 1% Mn-doped ZnO and **(c)** 5% Mn-doped ZnO

Table 3 Mean results of minimum inhibitory concentration tests for *S. aureus* and *B. subtilis* against the undoped ZnO, 1% Mn-doped ZnO and 5% Mn-doped ZnO at concentrations of 25 mg/mL, 50 mg/mL, 100 mg/mL, 250 mg/mL and 500 mg/mL

Bacteria strain	Sample	Average (±SD) zone of inhibition/mm				
		25 mg/mL	50 mg/mL	100 mg/mL	250 mg/mL	500 mg/mL
B. subtilis	ZnO	8.5 (±0.5)	9.0 (±1.0)	12.7 (±1.2)	10.0 (±1.0)	10.0 (±0.0)
	1% Mn-doped ZnO	13.7 (±0.6)	15.3 (±0.6)	14.0 (±1.0)	12.3 (±2.5)	13.3 (±2.1)
	5% Mn-doped ZnO	13.7 (±2.5)	13.3 (±1.2)	11.3 (±1.5)	11.2 (±0.3)	11.8 (±1.0)
S. aureus	ZnO	8.0 (±1.7)	11.0 (±1.0)	9.3 (±1.2)	8.3 (±1.2)	8.3 (±1.2)
	1% Mn-doped ZnO	8.0 (±0.5)	8.8 (±1.3)	10.3 (±1.5)	9.5 (±0.9)	9.3 (±0.8)
	5% Mn-doped ZnO	8.5 (±0.9)	9.0 (±0.5)	9.7 (±1.2)	9.2 (±0.3)	9.7 (±0.6)

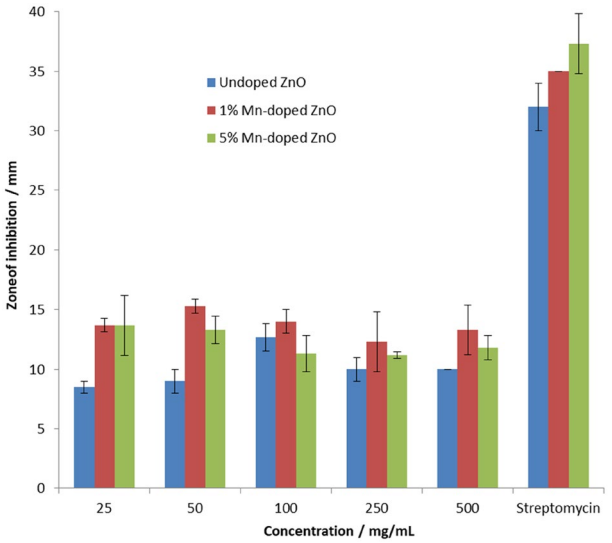

Fig. 9 Bar graph representing the zone of inhibition against concentration of Gram-positive *B. subtilis* for the green-synthesized ZnO, 1% Mn-doped ZnO and 5% Mn-doped ZnO

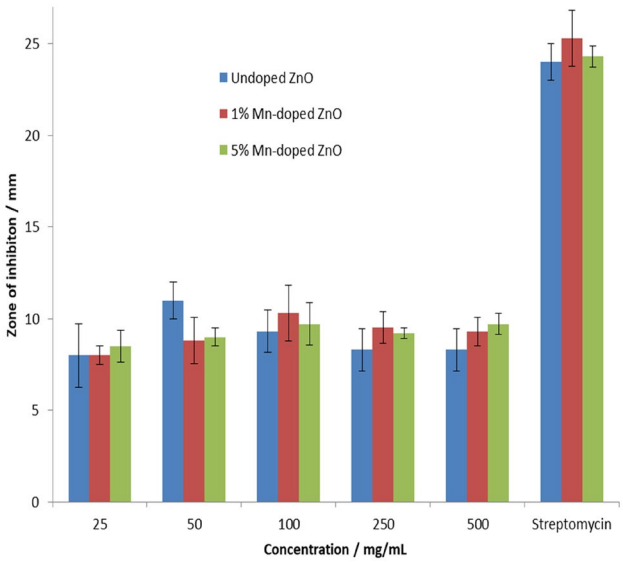

Fig. 10 Bar graph representing the zone of inhibition against concentration of Gram-positive *S. aureus* for biosynthesized ZnO, 1% Mn-doped ZnO and 5% Mn-doped ZnO

observed for the negative control. The zone of inhibition for the positive control, streptomycin was higher when compared to the ZnO, 1% Mn-doped ZnO and 5% Mn-doped ZnO.

The *B. subtilis* showed the highest zone of inhibition against 1% Mn-doped ZnO at 50 mg/mL. This was followed by 100 mg/ml of 1% Mn-doped ZnO, 25 mg/mL of 1% Mn-doped ZnO and 25 mg/mL of 5% Mn-doped ZnO where

Table 4 Tukey's HSD test for significant difference between streptomycin, ZnO, 1% Mn-doped ZnO and 5% Mn-doped ZnO for *B. subtilis*

Tested pair	Tukey HSD *p* value	Tukey HSD inference
Streptomycin vs ZnO	0.0010053	$p < 0.01$
Streptomycin vs 1% Mn-doped ZnO	0.0010053	$p < 0.01$
Streptomycin vs 5% Mn-doped ZnO	0.0010053	$p < 0.01$
ZnO vs 1% Mn-doped ZnO	0.0255702	$p < 0.05$
ZnO vs 5% Mn-doped ZnO	0.1212919	Insignificant
1% Mn-doped ZnO vs 5% Mn-doped ZnO	0.8081093	Insignificant

Table 5 Tukey's HSD test for significant difference between streptomycin, ZnO, 1% Mn-doped ZnO and 5% Mn-doped ZnO for *S. aureus*

Tested pair	Tukey HSD *p* value	Tukey HSD inference
Streptomycin vs ZnO	0.0010053	$p < 0.01$
Streptomycin vs 1% Mn-doped ZnO	0.0010053	$p < 0.01$
Streptomycin vs 5% Mn-doped ZnO	0.0010053	$p < 0.01$
ZnO vs 1% Mn-doped ZnO	0.1051034	Insignificant
ZnO vs 5% Mn-doped ZnO	0.1453654	Insignificant
1% Mn-doped ZnO vs 5% Mn-doped ZnO	0.8999947	Insignificant

both had the same zone of inhibition diameters (Table 3). For *S. aureus*, ZnO recorded the highest zone of inhibition at 50 mg/mL followed by 100 mg/mL of 1% Mn-doped ZnO. The 5% Mn-doped ZnO recorded the lowest value of the zone of inhibition between 8.5 and 9.7 mm for the range of concentrations tested.

As seen in Figs. 9 and 10, the toxicity of the green and phytogenic fabricated ZnO was comparatively low in comparison to the positive control. This difference between the biosynthesized ZnO and the positive control, streptomycin was significantly different with $p < 0.01$ (Tables 4 and 5).

The lower toxicity of the green-synthesized ZnO could be due to the agglomeration and aggregation of the particles which prevents the NPs from penetrating inside the bacteria effectively due to the submicron size and the lack of homogeneity [22]. This aggregation of ZnO could have raised due to the ZnO being nearly insoluble in water and the high polarity of the water which causes the ZnO to agglomerate [23].

The 1% Mn-doped ZnO was found to have a higher antibacterial activity for *B. subtilis* compared to the undoped ZnO ($p < 0.05$) (Table 4) in contrast to *S. aureus* (Table 5). This supports the theory by Mishra et al. [11] which suggests that the lower the band gap energy, the higher the antibacterial effect [4]. In addition to this, the 1% Mn-doped ZnO had the most positive zeta potential charge in comparison to the other biosynthesized ZnO. The higher positive zeta potential of 1% Mn-doped ZnO is suggested to have interacted with the negative surface potential of bacterial membrane which leads to shifting of potential towards surface charged neutrality that altered the membrane permeability or disrupted the membrane structure and results in bacterial inhibition [24].

Conclusion

A green and phytogenic method was successfully used to fabricate undoped ZnO, 1% and 5% Mn-doped ZnO using aqueous leaf extract of *M. malabathricum* plant which was confirmed by powder XRD, XPS, SEM, and EDX. Powder XRD and XPS confirmed the wurtzite structure of the materials and the oxidation state of both Zn and Mn was found to be + 2. The zeta potential measurements showed that undoped ZnO has a net negative surface charge; whereas, the 1% and 5% Mn-doped ZnO have a net positive surface charge. The biosynthesized undoped ZnO, 1% and 5% Mn-doped ZnO showed no bacterial activity on the Gram-negative bacteria *P. aeruginosa* and *E. coli*. However, these fabricated NPs showed an antibacterial effect towards Gram-positive bacteria *S. aureus* and *B. subtilis*. The 1% Mn-doped ZnO was the most effective on *B. subtilis* with the minimum inhibitory concentration being 50 mg/mL.

Acknowledgements Authors would like to acknowledge the FIC block grant UBD/RSCH/1.4/FICBF(b)/2018/012 received from Universiti Brunei Darussalam, Brunei Darussalam. Authors would also like to thanks CAMES, UBD for extending their facilities for some analysis.

Compliance with ethical standards

Conflict of interest The authors declare no conflict of interest.

References

1. Demirel R, Suvacı E, Şahin İ, Dağ S, Kılıç V (2018) Antimicrobial activity of designed undoped and doped MicNo-ZnO particles. J Drug Deliv Sci Technol 47:309–321. https://doi.org/10.1016/j.jddst.2018.07.024
2. Dobrucka R, Długaszewska J (2016) Biosynthesis and antibacterial activity of ZnO nanoparticles using *Trifolium pratense* flower extract. Saudi J Biol Sci 23:517–523. https://doi.org/10.1016/j.sjbs.2015.05.016
3. Bui V, Park D, Lee Y-C (2017) Chitosan combined with ZnO, TiO_2 and Ag nanoparticles for antimicrobial wound healing applications: a mini review of the research trends. Polymers (Basel) 9:21. https://doi.org/10.3390/polym9010021
4. Kundu D, Hazra C, Chatterjee A, Chaudhari A, Mishra S (2014) Extracellular biosynthesis of zinc oxide nanoparticles using *Rhodococcus pyridinivorans* NT2: Multifunctional textile finishing, biosafety evaluation and in vitro drug delivery in colon carcinoma. J Photochem Photobiol B Biol 140:194–204. https://doi.org/10.1016/j.jphotobiol.2014.08.001
5. Arakha M, Roy J, Nayak PS, Mallick B, Jha S (2017) Zinc oxide nanoparticle energy band gap reduction triggers the oxidative stress resulting into autophagy-mediated apoptotic cell death. Free Radic Biol Med 110:42–53. https://doi.org/10.1016/j.freeradbiomed.2017.05.015
6. Zhang Y, Nguyen KC, Caldwell D, Fine JH, Lefebvre DE, Tayabali AF (2017) Immune responses during single and repeated murine endotracheal exposures of zinc oxide nanoparticles. NanoImpact 7:54–65. https://doi.org/10.1016/j.impact.2017.06.003
7. Ahtzaz S, Nasir M, Shahzadi L, Amir W, Anjum A, Arshad R, Iqbal F, Chaudhry AA, Yar M, ur Rehman I (2017) A study on the effect of zinc oxide and zinc peroxide nanoparticles to enhance angiogenesis-pro-angiogenic grafts for tissue regeneration applications. Mater Des 132:409–418. https://doi.org/10.1016/j.matdes.2017.07.023
8. Moontragoon P, Pinitsoontorn S, Thongbai P (2013) Mn-doped ZnO nanoparticles: preparation, characterization, and calculation of electronic and magnetic properties. Microelectron Eng 108:158–162. https://doi.org/10.1016/j.mee.2013.01.061
9. Zare E, Pourseyedi S, Khatami M, Darezereshki E (2017) Simple biosynthesis of zinc oxide nanoparticles using nature's source, and it's in vitro bio-activity. J Mol Struct 1146:96–103. https://doi.org/10.1016/j.molstruc.2017.05.118
10. Dumbrava A, Berger D, Matei C, Radu MD, Gheorghe E (2018) Characterization and applications of a new composite material obtained by green synthesis, through deposition of zinc oxide onto calcium carbonate precipitated in green seaweeds extract. Ceram Int 44:4931–4936. https://doi.org/10.1016/j.ceramint.2017.12.084
11. Mishra PK, Mishra H, Ekielski A, Talegaonkar S, Vaidya B (2017) Zinc oxide nanoparticles: a promising nanomaterial for biomedical applications. Drug Discov Today 22:1825–1834. https://doi.org/10.1016/j.drudis.2017.08.006
12. Ehsan S, Sajjad M (2017) Bioinspired synthesis of zinc oxide nanoparticle and its combined efficacy with different antibiotics against multidrug resistant bacteria. J Biomater Nanobiotechnol 08:159–175. https://doi.org/10.4236/jbnb.2017.82011
13. Nagajyothi PC, Cha SJ, Yang IJ, Sreekanth TVM, Kim KJ, Shin HM (2015) Antioxidant and anti-inflammatory activities of zinc oxide nanoparticles synthesized using *Polygala tenuifolia* root extract. J Photochem Photobiol B Biol 146:10–17. https://doi.org/10.1016/j.jphotobiol.2015.02.008
14. Khan MM, Saadah NH, Khan ME, Harunsani MH, Tan AL, Cho MH (2019) Potentials of *Costus woodsonii* leaf extract in producing narrow band gap ZnO nanoparticles. Mater Sci Semicond Process 91:194–200. https://doi.org/10.1016/j.mssp.2018.11.030
15. Khan MM, Saadah NH, Khan ME, Harunsani MH, Tan AL, Cho MH (2019) Phytogenic synthesis of band gap-narrowed ZnO nanoparticles using the bulb extract of *Costus woodsonii*. Bionanoscience 9:334–344. https://doi.org/10.1007/s12668-019-00616-0
16. Ansari SA, Khan MM, Kalathil S, Nisar A, Lee J, Cho MH (2013) Oxygen vacancy induced band gap narrowing of ZnO nanostructures by an electrochemically active biofilm. Nanoscale 5:9238. https://doi.org/10.1039/c3nr02678g
17. Joffry SM, Yob NJ, Rofiee MS, Affandi MMRMM, Suhaili Z, Othman F, Akim AM, Desa MNM, Zakaria ZA (2012) *Melastoma malabathricum* (L.) smith ethnomedicinal uses, chemical constituents, and pharmacological properties: a review, evidence-based complement. Altern Med 2012:1–48. https://doi.org/10.1155/2012/258434
18. Lohézic-Le Dévéhat F, Bakhtiar A, Bézivin C, Amoros M, Boustie J (2002) Antiviral and cytotoxic activities of some Indonesian plants. Fitoterapia 73:400–405. https://doi.org/10.1016/S0367-326X(02)00125-9
19. Raj LFA, Jayalaskhmy E (2015) Biosynthesis and characterization of zinc oxide nanoparticles using root extract of *Zingiber Officinale*. Orient J Chem 31:51–56. https://doi.org/10.13005/ojc/310105
20. Moezzi A, McDonagh AM, Cortie MB (2012) Zinc oxide particles: synthesis, properties and applications. Chem Eng J 185–186:1–22. https://doi.org/10.1016/j.cej.2012.01.076
21. Gonzalez MR, Ducret V, Leoni S, Perron K (2019) *Pseudomonas aeruginosa* zinc homeostasis: key issues for an opportunistic pathogen. Biochim Biophys Acta Gene Regul Mech 1862:722–733. https://doi.org/10.1016/j.bbagrm.2018.01.018
22. Saravanan M, Gopinath V, Chaurasia MK, Syed A, Ameen F, Purushothaman N (2018) Green synthesis of anisotropic zinc oxide nanoparticles with antibacterial and cytofriendly properties. Microb Pathog 115:57–63. https://doi.org/10.1016/j.micpath.2017.12.039
23. Dimapilis EAS, Hsu CS, Mendoza RMO, Lu MC (2018) Zinc oxide nanoparticles for water disinfection. Sustain Environ Res 28:47–56. https://doi.org/10.1016/j.serj.2017.10.001
24. Arakha M, Saleem M, Mallick BC, Jha S (2015) The effects of interfacial potential on antimicrobial propensity of ZnO nanoparticle. Sci Rep 5:9578. https://doi.org/10.1038/srep09578